RESEARCH ARTICLE

Synthesis of zeolite-doped polyaniline composite for photocatalytic degradation of methylene blue from aqueous solution

Veena Sodha[1] · Hardik Koshti[1] · Rama Gaur[1] · Irfan Ahmad[2] · Rajib Bandyopadhyay[1] · Syed Shahabuddin[1]

Abstract

The generation of wastewater has increased rapidly with the expansion of industries, hence, posing a risk to human health and the environment. The development of novel materials and technologies for textile wastewater treatment is constantly evolving. In this work, the photocatalytic degradation of methylene blue employing ZSM-5 zeolite-doped polyaniline composites is presented. To fabricate ZSM-5-based polyaniline (PANI) composites, the simple approach of in situ oxidative polymerization has been adopted. Different weight ratios of ZSM-5 have been used for the synthesis, and samples have been labelled as PAZe-1, PAZe-5, and PAZe-10. Different characterization techniques were used to characterize the prepared composites, including field-emission scanning electron microscope (FESEM), transmission electron microscope (TEM), Fourier transform infrared (FT-IR), X-ray diffraction (XRD), and thermo-gravimetry analysis (TGA). The photocatalytic performance of polyaniline, ZSM-5, and their composites was assessed by monitoring the degradation of methylene blue in the presence of visible light. Degradation results of the polyaniline-doped composites were found to be better than that of the polyaniline alone. When the photocatalytic efficiencies of different composites were compared, the PAZe-1 showed the best performance, with 99.9% degradation efficiency after 210 min of irradiation, while PANI, PAZe-5, PAZe-10, and ZSM-5 show 38%, 82%, 71%, and 99% removal efficiency. Apart from methylene blue, the composite PAZe-1 was further explored for the degradation of other organic pollutants such as methyl orange, chlorpyrifos, 2,4-dichlorophenoxy acetic acid, and p-nitroaniline. To determine the reactive species involved in the photocatalysis mechanism, scavenger studies were performed.

Keywords Zeolite · Polyaniline · Photocatalysis · Methylene blue · Composite

Introduction

Freshwater is something that every living creature needs to survive. A large amount of industrial trash is discharged into water sources daily (Darban et al. 2022). The issue related to wastewater must be addressed immediately since the contaminants present in the wastewater are harmful to humans, aquatic life, and the environment. Many approaches,

including adsorption (Jha et al. 2022) (Delanka-Pedige et al. 2022; Sessarego et al. 2019), photocatalysis (Alberti et al. 2021; Shkir et al. 2022; Younis et al. 2021), coagulation (Domingues et al. 2021), ion-exchange (Ownby et al. 2021), and filtration (Gupta et al. 2021), have been employed to treat effluents in wastewater. Both adsorption and photocatalysis have been widely applied in the treatment of organic pollutants. Materials such as zeolites (Alswat et al. 2016, Armağan and Turan 2004), chitosan (Mehmood et al. 2020; Shahabuddin et al. 2015), and rice straw sourced biochar (Li et al. 2021; Mehmood et al. 2022, 2021) have been used for the adsorption and immobilization purposes in various applications. Though in the adsorption processes, the pollutants are just extracted from wastewater, and the disposal of the used adsorbent itself is a matter of concern. Photocatalysis, on the other hand, is an economically viable, time-saving technique that degrades the pollutant with no secondary contamination. In the current research, a composite material of zeolite and conducting polymer is employed for the

✉ Syed Shahabuddin
syedshahab.hyd@gmail.com

1 Department of Chemistry, School of Energy Technology, Pandit Deendayal Energy University, Knowledge Corridor, Raisan, Gandhinagar 382426, Gujarat, India

2 Department of Clinical Laboratory Sciences, College of Applied Medical Sciences, King Khalid University, Abha 61421, Saudi Arabia

degradation of methylene blue and other organic pollutants such as chlorpyrifos, methyl orange, 2,4-dichlorophenoxy acetic acid, and p-nitroaniline.

Zeolites are crystalline solids of aluminosilicates having microporous pore sizes, i.e. < 10 Å. Zeolites possess multifunctional properties such as high surface area, high thermal stability, precise microporosity, high adsorption efficiency, and are suitable for catalysis. In the field of wastewater treatment, zeolites are broadly utilized as adsorbents (Tagliabue et al. 2012) and ion-exchangers (Alshameri et al. 2014). Zeolites have a negatively charged framework and methylene blue being a cationic dye easily gets attracted to them. The interaction of zeolites with water contaminants is mostly through physical forces, which are not as strong as chemical interactions, and there is a possibility of desorption. Hence, the process needs to be improved. Photodegradation involves photocatalysis, a chemical process, in which active oxygen species (AOS) are generated which degrade the organic contaminants. One of the disadvantages of photocatalysis is that most of the photocatalysts used have low adsorption potential, which can be readily overcome by introducing zeolites. The composite materials exhibit both adsorption and photocatalysis; when coupled with zeolites, even if the interactions are weak, the pollutants adsorbed on the surface of zeolite will be completely degraded by the photoactive component.

ZnO (Liu et al. 2021b), CdS (Tayyab et al. 2022b), Mxene (Tayyab et al. 2022a), and carbon-based materials (Liu et al. 2021a) are well-known photocatalysts and have been explored for various applications such as photodegradation, photoreduction. and H_2 production.

Currently, zeolite photochemistry only involves the practice of zeolites as a host molecule and not as the photocatalyst (Alvarez-Aguinaga et al. 2020). Research is more focused on incorporating a photoactive agent in the zeolite nanopores for the synthesis of "zeolite-based photocatalysts" (Alvarez-Aguinaga et al. 2020), while in this study, the bandgap of zeolite ZSM-5 has been measured and explained how ZSM-5 and polyaniline work synergistically. In addition, when zeolites are used in the form of their composites, they show better physiochemical stability, higher adsorption capacity, and easier reusability which is rare while working with zeolites.

Due to its fascinating qualities such as cost-effectiveness, chemical stability, and facile synthesis, polyaniline (PANI) is a unique and amazing candidate from the conducting polymer class (Parekh et al. 2022). Also, upon visible light excitation, PANI can donate the electrons and act as a good hole transporter (Shahabuddin et al. 2016), though the electron–hole recombination hinders its efficiency, which can be overcome via doping of other semiconducting material (Shahabuddin et al. 2016).

In present research, the photocatalyst material has been prepared by doping ZSM-5 with polyaniline via in situ oxidative polymerization. Polyaniline, a conducting polymer, was chosen as it is cost-effective, easy to synthesize, and has high electron–hole mobility. ZSM-5 was synthesized via conventional hydrothermal treatment and then integrated into the polymeric matrix during polymerization (Zhou et al. 2013). Morphological analysis, structural analysis, and photo-responsive properties were studied for the synthesized composites and parent materials. For the photodegradation studies, methylene blue was used as a model dye, and degradation was performed under the visible light source. By doping ZSM-5 in different weight ratios, both polyaniline and ZSM-5 worked synergistically, and the electron–hole recombination was reduced significantly in PANI. Furthermore, the cationic dye methylene blue easily adheres to the surface of composite as ZSM-5 has a negative charge which speeds up the overall degradation. The photocatalytic behaviour of composites with different weight percentage loading of ZSM-5 was analysed. The composite material was also explored for the degradation of some other organic pollutants. To understand the underlying photocatalytic mechanism, scavenger studies were performed.

Experimental section

Materials

Aniline (Sigma Aldrich, 99%) used was distilled at reduced pressure and kept in the dark before use. Other chemicals, such as colloidal silica (commercial grade, 30%), sodium aluminate (Sigma Aldrich, 56.15% Al_2O_3, 43.9% Na_2O), tetra propyl ammonium hydroxide (TPAOH) (commercial grade, 40%), ammonium peroxydisulfate (APS) (sigma Aldrich, 98%), HCl (Merck, 37.5%), methanol (Finar, 99.8%), and acetone (Finar, 99.5%), were used as received. Throughout the study, distilled water was utilized for different experiments.

Preparation of ZSM-5

ZSM-5 was synthesized via traditional method of hydrothermal treatment as described in Zhou et al. (2013) with modification. Firstly, sodium aluminate was separately dissolved in deionized water. Colloidal silica and tetrapropyl ammonium hydroxide (TPAOH) were then added to the above solution drop wise as per the batch composition $30SiO_2:Al_2O_3:1.35Na_2O:6.54TPAOH:900H_2O$. The reaction was continuously stirred at 60℃ for 24 h to make a homogenous mixture. Synthesized gel was then transferred to a Teflon-lined autoclave and hydrothermally treated at

160℃ for 48 h. The obtained product was filtered using vacuum filtration, washed, and dried in the oven at 120℃.

Preparation of polyaniline

The oxidative polymerization method was performed to synthesize polyaniline. In the first step, distilled aniline (0.0536 mol) was dissolved in 74 ml 1 M HCl. The oxidant solution was prepared by dissolving ammonium persulphate (APS) (0.0671 mol) in 88 ml 1 M HCl then added drop wise into the previously prepared aniline solution. The reaction mixture was stirred continuously for 2–3 h at 0–5℃. Subsequently, the reaction mixture was filtered and washed using 0.5 M HCl until the filtrate was colourless, followed by distilled water until the filtrate was neutral (Shahabuddin et al. 2015).

Preparation of polyaniline-zeolite composite

Conducting polymer-based zeolite composites were synthesized by taking various wt% of ZSM-5 with respect to aniline, i.e. 1%, 5%, and 10%. A known amount of ZSM-5 was dispersed in 5 ml 1 M HCl by sonication. Solution of distilled aniline in 1 M HCl is added into zeolitic dispersion slowly with vigorous stirring. The subsequent reaction workup is as stated in the preceding section. Sample codes PAZe-1, PAZe-5, and PAZe-10 were assigned to the composites that included 1, 2, and 5 wt% loading of ZSM-5 with respect to aniline, respectively.

Characterization techniques

Powder X-ray diffraction pattern (P-XRD) of all the samples were recorded using PANalytical X'Pert Pro diffractometer at 30 mA and 40 kV using filtered Cu Kα radiation ($\lambda = 1.54184$ Å). XRD patterns were recorded over a 2θ range of 5 to 50 degrees with a goniometer speed and step size of 1° per minute. Thermal analysis was performed on HITACHI STA7200 for thermogravimetric analysis. The heating rate was 10℃/min under air flow (99.99%) or nitrogen (99.99%) of 20 ml min^{-1}. The final temperature was 900 ℃. The surface morphological analysis of the samples was done via field emission scanning electron microscope (FE-SEM) using Zeiss Ultra 55 instruments and transmission electron microscope (TEM) using JEOL JEM-F200 KV Gatan Digital Micrograph (GDM). Prior to the FE-SEM analysis, all the samples were coated with a thin gold layer by using LEICA EM ACE200 to make the sample conductive.

FTIR spectra were recorded with Perkin Elmer spectrum II FT-IR spectrometer in the region of 4000 – 400 cm^{-1} with. In order to improve signal-to-noise ratio, 10 scans per minute were performed, and data are treated with the spectrum for windows software. Absorbance spectra of samples were obtained by UV/VIS spectrometer, in the 200–800 nm range LABINDIA analytical model UV 3000^{+}. Diffuse reflectance spectra of ZSM-5 were recorded on UV/VIS spectrometer, PerkinElmer model Lambda 35.

Photocatalytic dye degradation study

The photocatalytic activities of the synthesized samples were examined by monitoring the methylene blue (MB) dye degradation in the aqueous phase. In a quartz vessel, 25 mg of prepared photocatalyst were dispersed in 50 ml of dye solution with 10mgL^{-1} initial concentration. Adsorption–desorption equilibrium was established by stirring the mixture in dark for 60 min. After that, 450-W HPMVL VIS lamp high-pressure lamp was used to irradiate the above mixture at a distance of 8 cm from the solution to perform photocatalytic degradation for 210 min. At different time intervals, 3 ml of the sample was withdrawn from the above suspension and centrifuged. The degradation was then analysed by taking UV–vis absorbance spectra of supernatant solutions (Shahabuddin et al. 2016). The optimized photocatalyst was then used for the degradation of p-nitroaniline, methyl orange, and agrochemicals, i.e. 2,4-dichlorophenoxyacetic acid and chlorpyrifos. For this study, 25 mg of optimized catalyst was dispersed in 50 ml contaminant solution of 10mgL^{-1} initial concentration. The mixture was then irradiated with 450-W HPMVL VIS lamp high-pressure lamp until the maximum degradation was achieved.

Results and discussion

XRD analysis

The XRD graphs of PANI, ZSM-5, and composite PAZe-10 are shown in Fig. 1. Polyaniline exhibits three prominent diffraction peaks at 2θ = 14.85°, 20.7°, and 25.4°, which are not sharp enough and indicate that polyaniline has polycrystalline nature. The periodic repetition of benzenoid and quinoid rings in the polyaniline structure is responsible for the diffraction peaks at 2θ = 20.7° and 25.4° (Shi et al. 2009). ZSM-5 shows characteristic sharp peaks at 2θ = 13.94°, 14.83°, 15.94°, 17.77°, 20.83°, 23.11°, 23.88°, 24.44°, 26.16°, 29.27°, 29.94°, 36.11°, and 45.38° with planes (130), (031), (022), (400), (−113), (051), (−303), (−133), (441), (352), (360), (470), and (941), respectively. From the XRD graph of composite PAZe-10, it is evident that the nature of the curve follows the pattern of polyaniline. All three peaks of polyaniline 2θ = 14.85°, 20.7°, and 25.4° are present in the curve of PAZe-10. In addition, four prominent peaks of ZSM-5 at 2θ = 23.05°, 28.66°, 29.83°, and 45.22° with planes (051), (352), (360), and (941), respectively, are also present. Hence, the XRD graph of PAZe-10 indicates the presence of ZSM-5
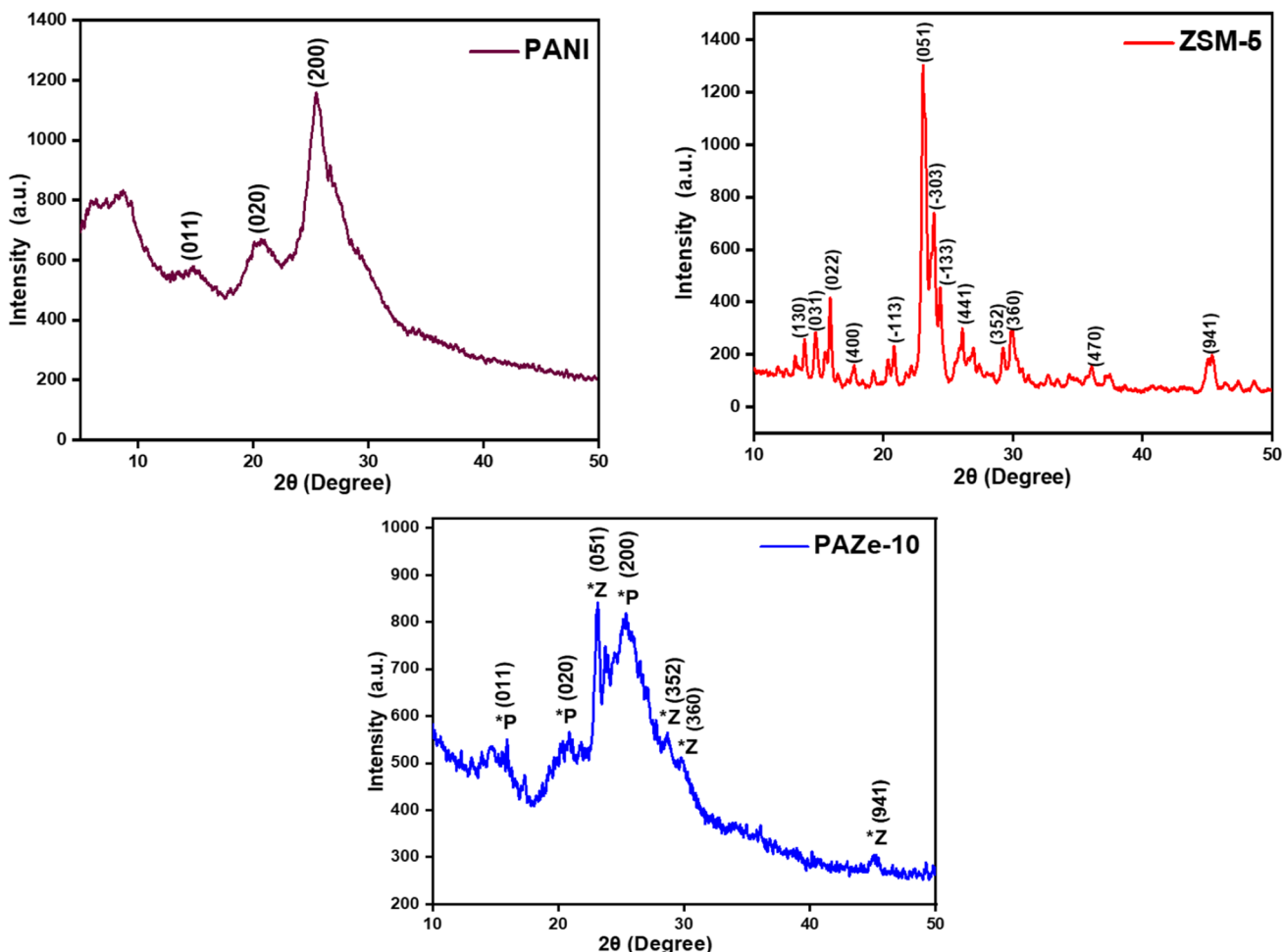
Fig. 1 X-ray diffraction graphs of ZSM-5, polyaniline, and composite PAZe-10

and PANI in the composite. The average crystallite sizes of ZSM-5 and PAZe-10 were calculated using the Scherrer equation as depicted in Khan et al. (2020) and Danish et al. (2020).

$$d = \frac{k\lambda}{\beta \cos \theta} \tag{1}$$

where,

λ wavelength of X-ray

k constant 0.9

β FWHM width of diffraction peak

θ angle of diffraction

The average crystallite size of ZSM-5 and PAZe-10 was calculated as 16.98nm and 5.91nm, respectively.

UV–vis analysis

Figure 2 shows UV-vis absorbance spectra of PANI, ZSM-5, PAZe-1, PAZe-5, and PAZe-10. PANI exhibits a characteristic absorption band at 505–780nm which shows it has a good ability to absorb light within the visible range. This band is attributed to pi-pi* transitions in PANI. From the UV graph of ZSM-5, it can be seen that it has not shown any band in the visible region. While in the case of three of the composites, these show light absorption similar to PANI. Hence, these absorb light and are suitable for effective dye degradation.

The optical bandgap of a compound can be calculated using a UV–vis spectroscopy. Either UV–vis absorbance or diffuse reflectance spectra can be used for this analysis. In the present study, diffuse reflectance spectra are used for the bandgap analysis.

The Tauc method assumes that absorption coefficient α may be expressed as Eq. (2):

Fig. 2 UV–vis absorbance spectra of PANI, ZSM-5, PAZe-1, PAZe-5, and PAZe-10
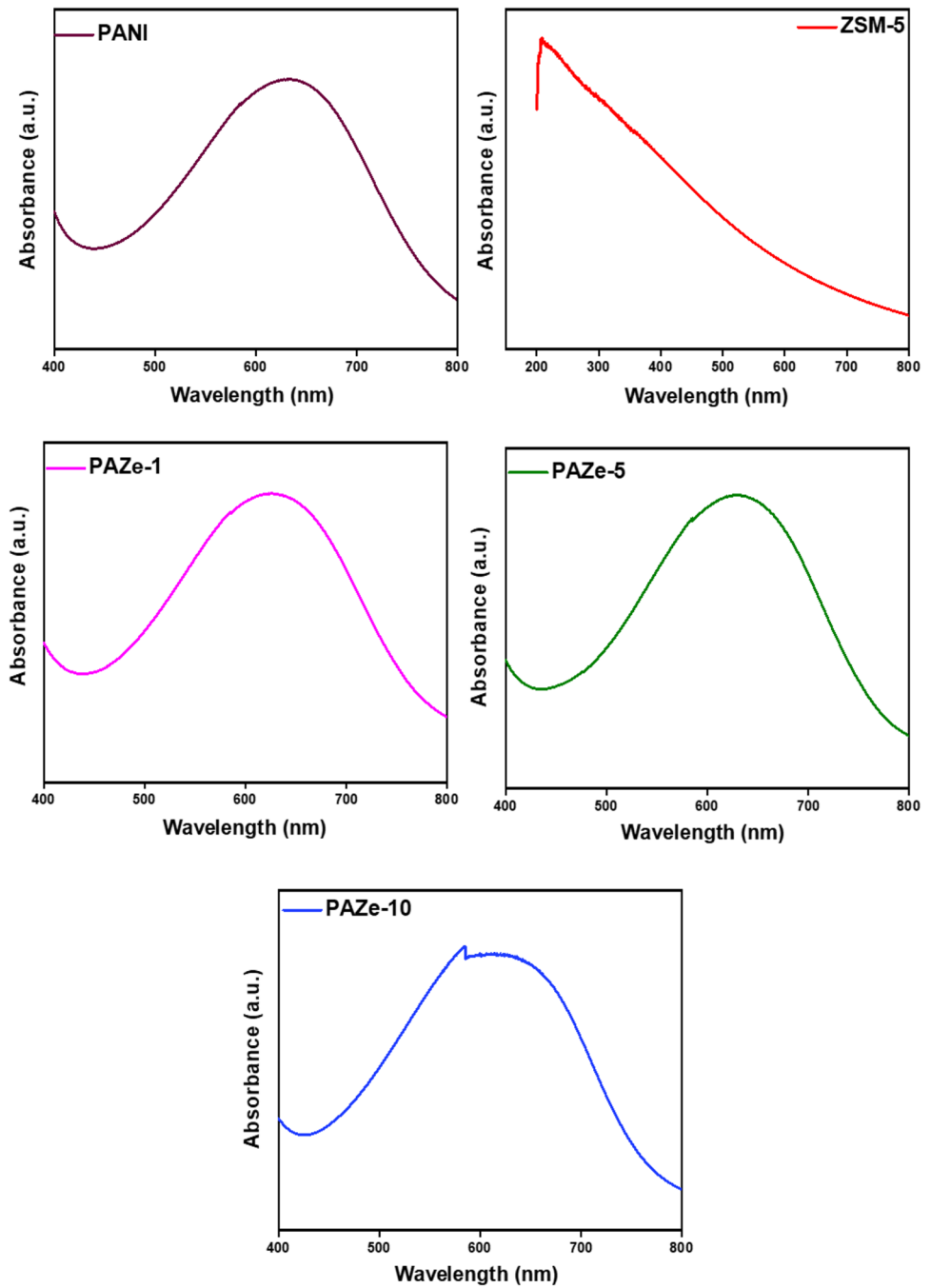
$$(\propto h\nu)^{\frac{1}{P}} = B(h\nu - E_g) \qquad (2)$$

where,

Eg   bandgap energy

B   constant

α   absorption coefficient

hν   energy of photon

P   ½ or 2 for direct and indirect bandgap.

First, the Kubelka–Munk function was applied to diffuse reflectance spectra of ZSM-5 to get its corresponding absorption spectra. The relation between absorption coefficient and reflectance given by Paul Kubelka and Franz Munk is as Eq. (3).

$$\propto = \frac{(1-R)^2}{2R} \tag{3}$$

Combining Eqs. (2) and (3), we get,

$$\left(\frac{(1-R)^2 h\nu}{2R}\right)^{\frac{1}{p}} = B((h\nu - E_g) \tag{4}$$

The diffuse reflectance spectra were transformed using Eq. (4) and plotted against photon-energy ($h\nu$) as shown in Fig. 3. The bandgap of ZSM-5 was estimated by extra plotting the tangent from the curve on X-axis (Makuła et al. 2018). The bandgap of ZSM-5 as estimated from the Tauc plot is found to be 2.73 eV.

FTIR analysis

The FTIR spectra of ZSM-5, polyaniline, and their composites are given in Fig. 4. In the FTIR spectrum of polyaniline, the distinctive peak at 1477 and 1568 cm^{-1} corresponds to C–C stretching vibrations of benzenoid and quinoid rings of polyaniline, respectively. The C-N and C$=$N stretching is indicated by the peak at 1292 cm^{-1}. N–H stretching modes are represented by a broad IR band at 3425 cm^{-1} (Shahabuddin et al. 2016). The characteristic peak at 1080 cm^{-1} in the FTIR spectrum of ZSM-5 represents -Si–O asymmetric stretching. The vibrational peaks at 790 cm^{-1} and 538 cm^{-1} attribute for -Al-O cm^{-1} and double ring vibration, respectively. For -Si–O bending, the peak is at 441 cm^{-1}. External links between TO_4 tetrahedral in the framework of ZSM-5 might be responsible for the peak at 1215 cm^{-1}. In the FTIR spectra of ZSM-5-doped polyaniline, the peak broadening
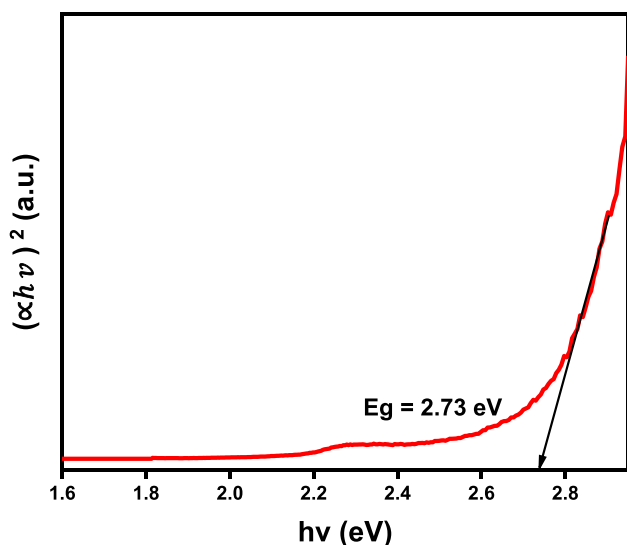
can be seen near 1106 cm^{-1} caused by the presence of -Si–O asymmetric stretching band of ZSM-5 as indicated by an arrow. Moreover, increasing the percentage loading of ZSM-5 raises the intensity of the Si–O asymmetric stretching band. Hence, based on reported literature and the data obtained with FTIR suggests that zeolite-doped polyaniline composites have been formed.

TGA analysis

Figure 5 demonstrates thermogravimetric curves of ZSM-5, PANI, PAZe-1, and PAZe-5. Thermal investigations of PANI, ZSM-5, PAZe-1, PAZe-5, and PAZe-10 were carried out within the temperature range of 35–900℃ and a 10℃/min heating rate in the presence of an inert N_2 atmosphere. According to the TGA curve of PANI, three big weight losses occurred between 35 and 900°C. Furthermore, the total weight loss observed is 86%. The first weight loss between 40 and 130°C might be because of the moisture loss, decomposition of impurities, and unreacted monomer molecules. The weight loss between 130 and 350℃ is possibly due to the loss of dopant materials. The weight reduction after 350℃ shows polymeric chain breakdown. The TGA curve of ZSM-5 shows a total weight loss of 12.8%, which is very less in comparison to polyaniline, which shows that ZSM-5 is thermally more stable than PANI. The slight weight loss in ZSM-5 below 300 is due to the loss of moisture. The ultimate weight loss at 300–550 °C is attributed to the elimination of organic template TPAOH (Narayanan et al. 2015). The TGA curve of composites follows the pattern of PANI as the concentration of PANI is high. From the TGA curves of PAZe-1 and PAZe-5, it is obvious that as the ZSM-5 doping increases, the thermal resistance of material increases. PAZe-1 and PAZe-5 experience 72.52% and 55.57% total decrease in weight, respectively. Hence, the thermal investigations indicate that doping of thermally stable ZSM-5 to PANI significantly increases the thermal stability of composite materials.

Morphological analysis

Morphological analysis of as-synthesized materials was accomplished via field emission scanning electron microscope (FE-SEM) and transmission electron microscope (TEM). Figure 6 shows the SEM images of PANI, ZSM-5, and PAZe-1 at different magnifications. FESEM images of polyaniline depict that it has tube-shaped particles with a smooth surface. The particles of ZSM-5 are spherically shaped, and the particle surface is slightly rough as shown in Fig. 7c–d. Morphological changes in PANI are observed by doping of ZSM-5. FESEM images of composite PAZe-1 show that as the

Fig. 3 Tauc plot of ZSM-5

Fig. 4 FTIR spectra of ZSM-5, PANI, and their composites PAZe-1, PAZe-5, and PAZe-10
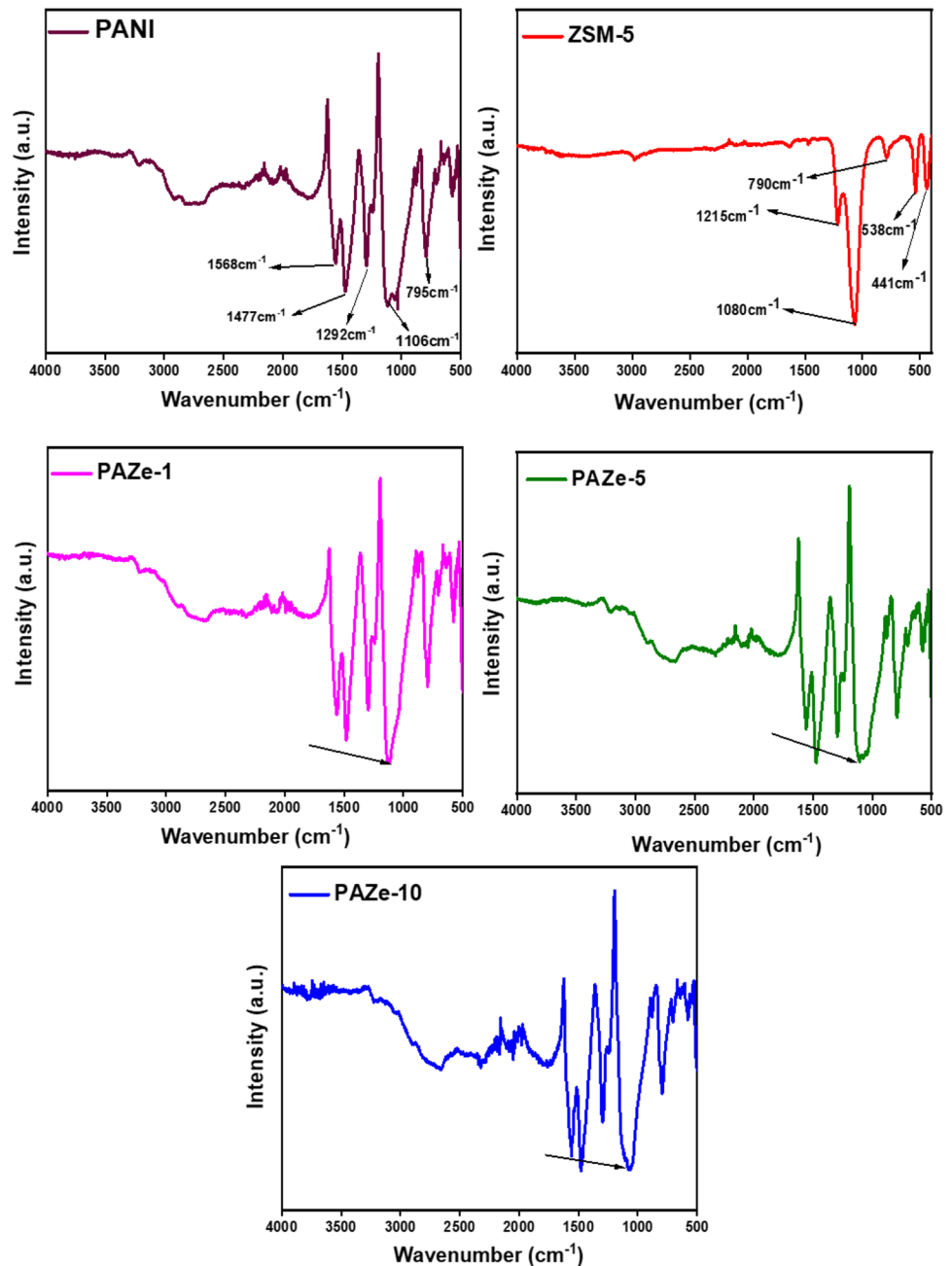
doping of ZSM-5 is very low, its particles have a tubular shape and rough surface. The slightly rough surface of PAZe-1 is due to the doping of ZSM-5 to PANI. The calculation of average particle size was done as depicted in Khan et al. (2020) using ImageJ software. The average particle size of ZSM-5 has been calculated as 188.24 nm as demonstrated in Fig S1. In the case of PANI and PAZe-1, the average tube diameter has been estimated as 75 nm and 80 nm respectively as demonstrated in Fig S2 and S3.

The formation of composite was also confirmed by performing the high-resolution transmission electron microscope (HRTEM) analysis of PAZe-1. Figure 7a and b show the HRTEM micrographs of PAZe-1 composite. The TEM image in Fig. 7a show the amorphous and crystalline regions in the composite material. The green arrow indicates the crystalline phases which are due to the presence of ZSM-5, and yellow arrow indicates the amorphous region indicating the presence of PANI in composite. This suggests the successful incorporation of crystalline ZSM-5 on the matrix of amorphous polyaniline. Furthermore, the TEM image in Fig. 7b shows the crystalline and amorphous phases of ZSM-5 and PANI, respectively, where the crystalline phase has been circled in red and amorphous in blue colour.
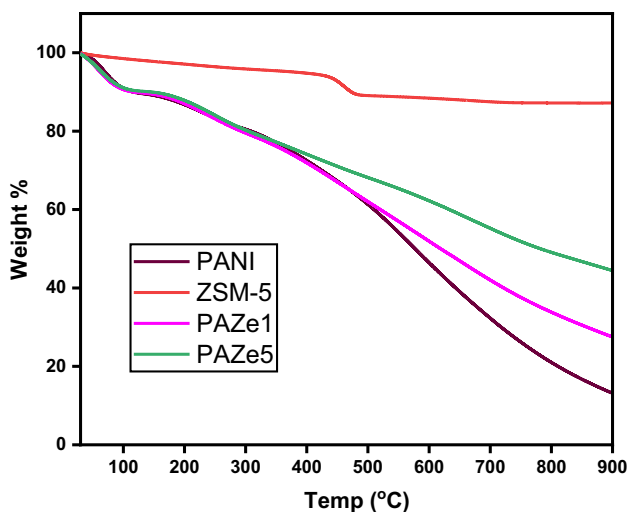
Fig. 5 Thermogravimetric curves of PANI, ZSM-5, PAZe-1, and PAZe-5

Figure 7c shows the SAED pattern of selected area in PAZe-1 composite, which gives characteristics reflection pattern of ZSM-5, which indicates that the synthesized zeolite possess high crystallinity and single crystalline nature (Narayanan et al. 2014).

Moreover, the TEM elemental mapping of PAZe-1 was also performed in order to find distribution of various elements in the composite. Figure 8 shows the elemental mapping images of PAZe-1. Figure 8b-g show the elemental mapping images of the composite, PAZe-1. The mapping analysis showed the uniform presence of C and N which confirms that the PANI is present in the composites uniformly. Also, the mapping depicts the presence of Si, Al, O, and Na which are due to the presence of ZSM-5 in the composite material (Akti and Okur 2018). The mapping analysis specified the presence of all the elements uniformly, thereby indicating the formation of a uniform composite material.

Fig. 6 FE-SEM images of **a**) and **b**) PANI, **c**) and **d**) ZSM-5, and **e**) and f) PAZe-1
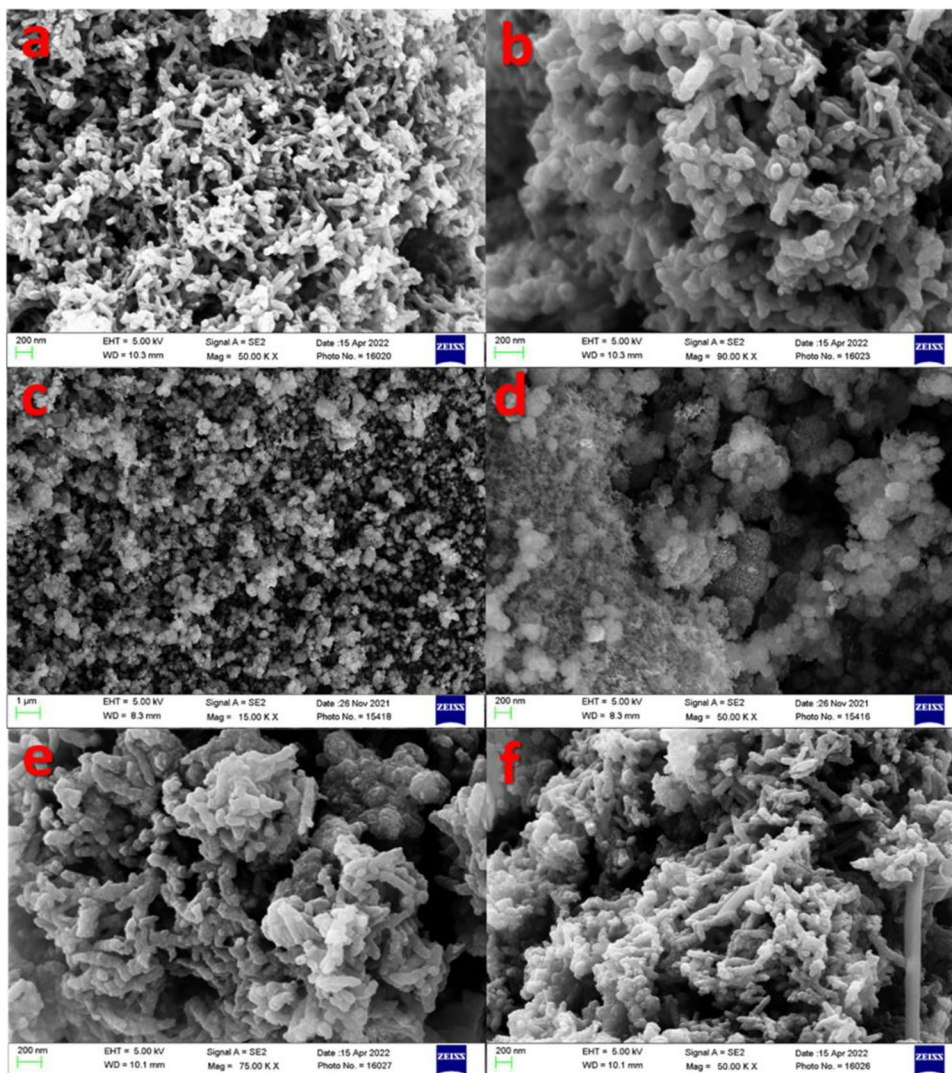
Fig. 7 (**a**) and (**b**) High-resolution transmission electron microscope (HRTEM) images of PAZe-1 composite. (**c**) SAED pattern of PAZe-1
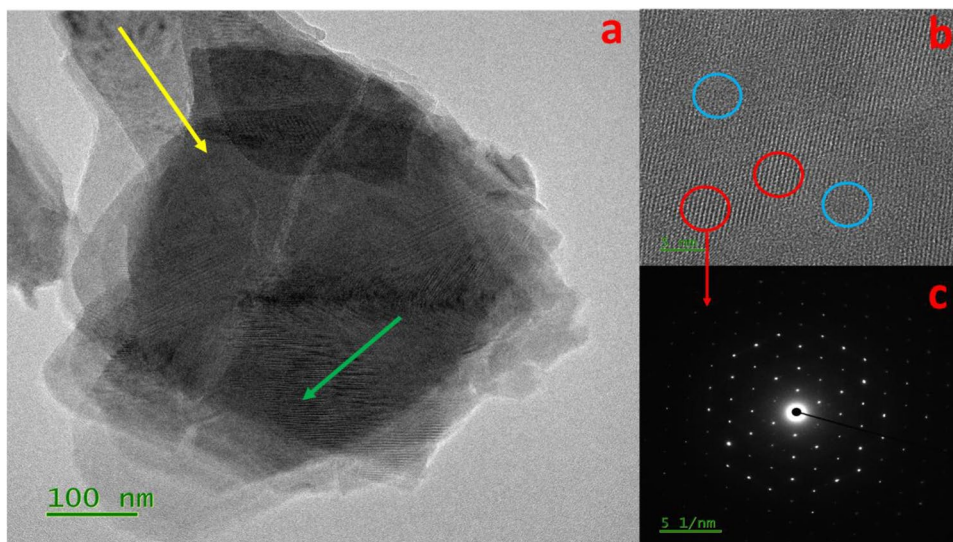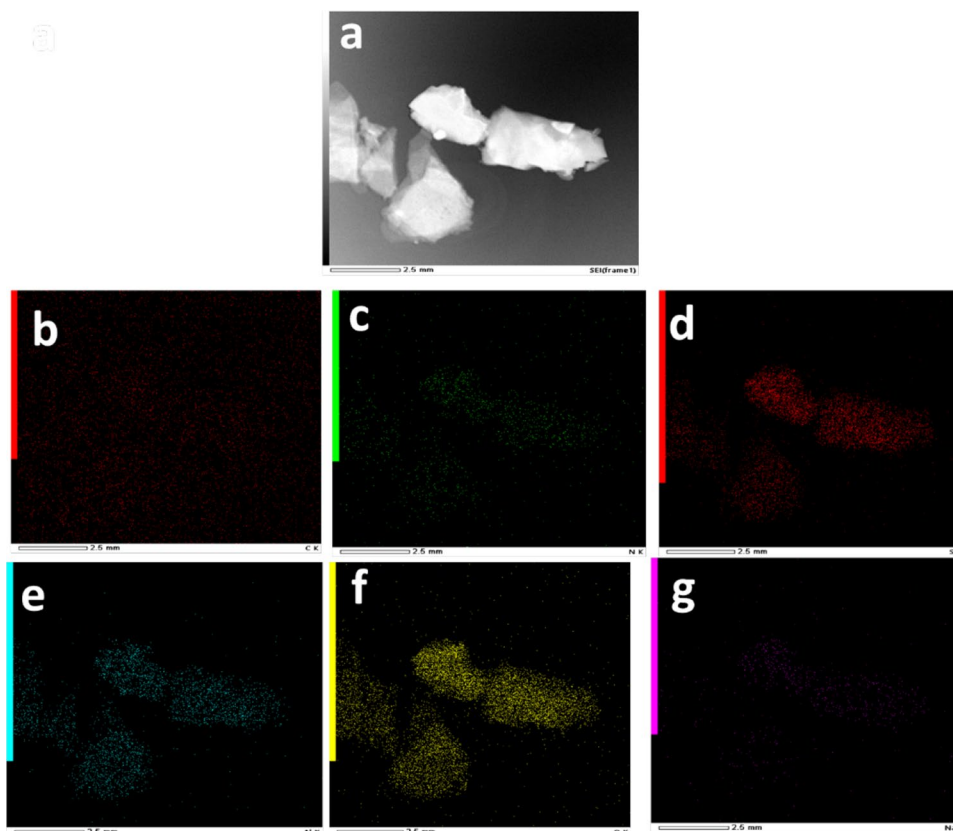

Fig. 8 (**a**) Elemental mapping images of PAZe-1 for the elements (**b**) C, (**c**) N, (**d**) Si, (**e**) Al, (**f**) O, and (**g**) Na
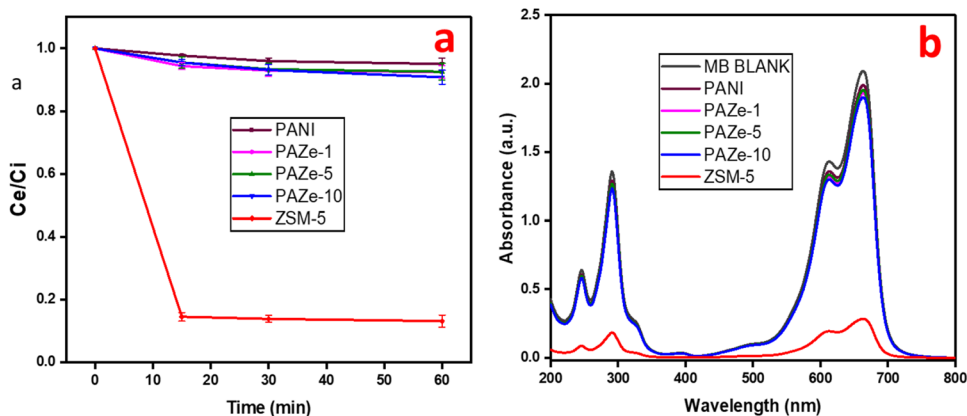

Photocatalytic degradation of MB in presence of visible light irradiations

Before performing the photocatalytic degradation, the mixture was stirred under the dark atmosphere to attain adsorption–desorption equilibrium as depicted in Fig. 9a, b. The percentage adsorbed by PANI, PAZe-1, PAZe-5, PAZe-10, and ZSM-5 was 4.9%, 7.6%, 6.7%, 9.2%, and 86%, respectively. The data shows that ZSM-5 has highest adsorption efficiency, and as the loading percentage of ZSM-5 in the composites increases, the adsorption efficiency increases.

To evaluate the photocatalytic efficiency of materials, right after the dark adsorption studies, photocatalytic degradation was carried out by irradiating the resultant mixture to visible light. The degradation was monitored at different

time intervals until 210 min. The photocatalytic degradation rate and % degradation of MB at various time intervals with several photocatalysts are shown in Fig. 10a, b. With a percentage degradation trend of PAZe-1 > PAZe-5 > PAZe-10 > PANI, it is clear that PANI has lower photocatalytic efficiency than PAZe-1, PAZe-5, and PAZe-10 composites. Figure 11 depicts the UV–vis absorption spectra of MB with PANI, ZSM-5, and three of their composites, i.e. PAZe-1, PAZe-5, and PAZe-10, at various time intervals. In the case of each photocatalyst, the intensity of the absorption band lowers as the light exposure period increases. For PANI, PAZe-1, PAZe-5, PAZe-10, and ZSM-5, the degradation percentages were 38%, 99%, 82%, 71%, and 99%, respectively, after 210 min of light irradiation.

Figure 12 shows the images of bare ZSM-5 as well as before and after adsorption. From these images, it can be seen that the colour of ZSM-5, which is white before adsorption, turns blue after adsorption due to adsorbed molecules of methylene blue on the surface of ZSM-5. Even after 210 min of photocatalysis, the colour of ZSM-5 is blue which indicates the presence of methylene blue dye on the surface of the adsorbent. Hence, it can be concluded that ZSM-5 gives adsorption not the photocatalysis. Figure 13a shows percentage adsorption bar graphs at 60 min of dark adsorption, and Fig. 12b shows the percentage degradation

bar graphs of PANI, PAZe-1, PAZe-5, PAZe-10, and ZSM-5 at 210 min of photocatalysis. From Fig. 13a, it can be observed that in absence of light, ZSM-5 has adsorbed 86% methylene blue. PANI, PAZe-1, PAZe-5, and PAZe-10 show very less adsorption efficiency for methylene blue. On the other hand, from Fig. 13b, it can be seen that that the composites have shown good photocatalytic response. The removal efficiency of PAZe-1, PAZe-5, and PAZe-10 has reached to 99%, 82%, and 71% from 7.6, 6.7, and 9.2 by light irradiation.

Mechanism

When exposed to the light of a certain wavelength, organic dyes can undergo electronic transitions and intersystem crossing resulting in the formation of singlet and triplet species. These species are highly reactive and readily interact with available oxygen and molecules to create active oxidizing species (AOS) such as peroxides, superoxide, and hydroxyl radicals. These AOSs are extremely responsive and target dyes and other organic pollutants and degrade them, though the rate of generation of AOS in methylene blue alone is low and required to be accelerated with support of a photo-responsive material. Polyaniline has a conjugated π system and can easily conduct the electrons. Similar to
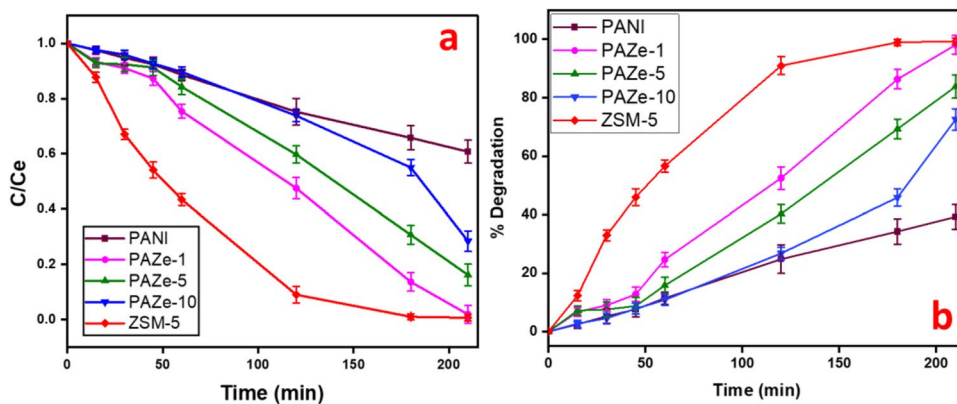
Fig. 11 Methylene blue UV–vis absorbance spectra in presence of different photocatalyst, i.e. (**a**) PANI, (**b**) ZSM-5, (**c**) PAZe-1, (**d**) PAZe-5, and (**e**) PAZe-10 after 210 min of photocatalytic degradation
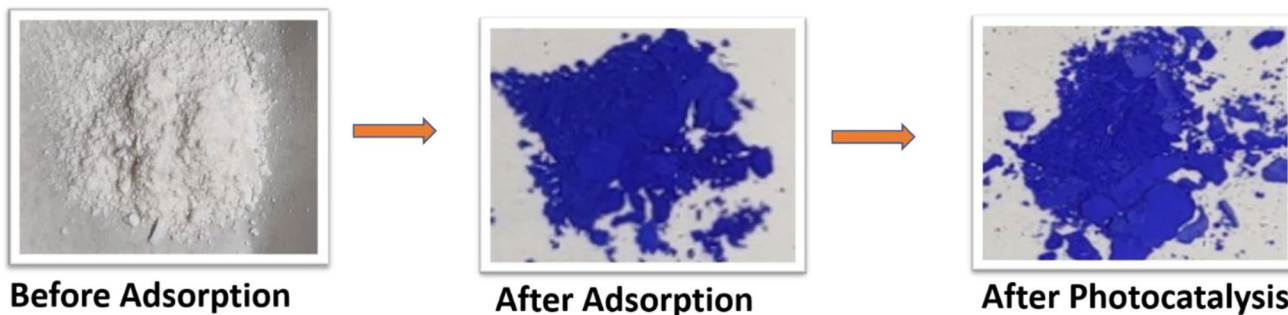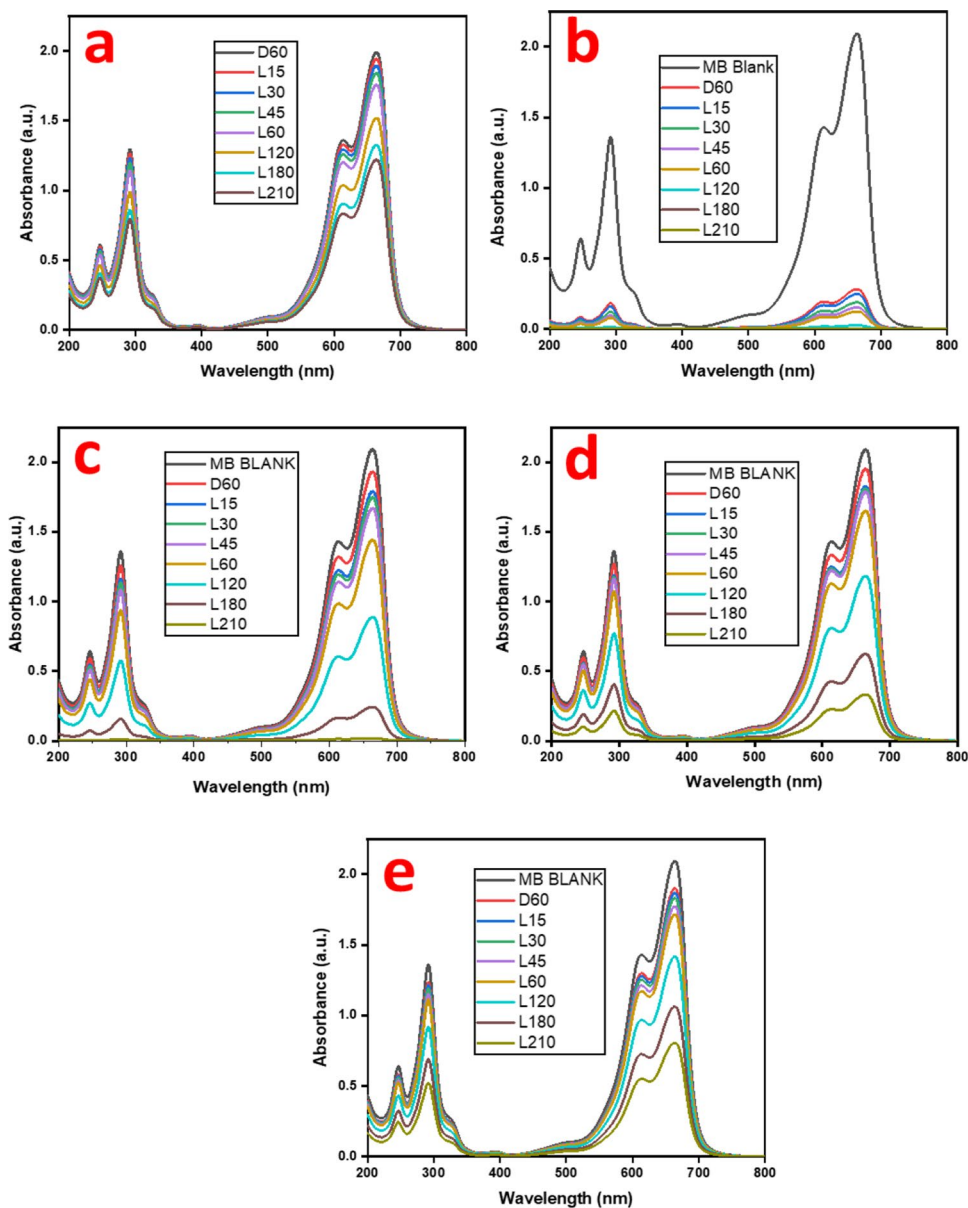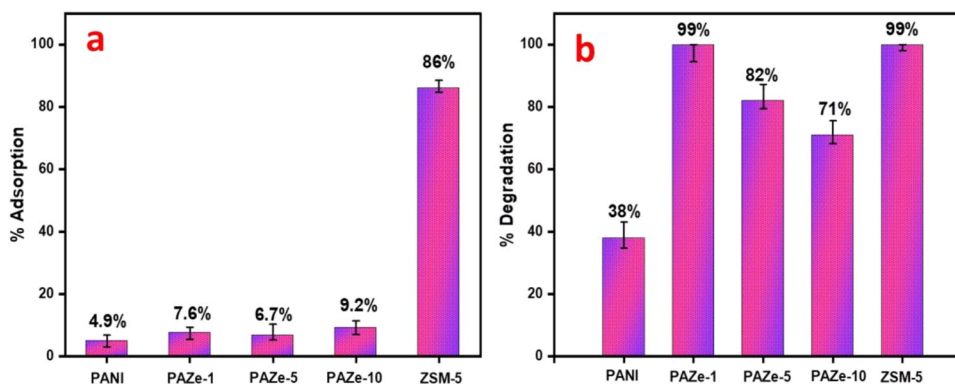

Fig. 12 Images of ZSM-5 before adsorption, after adsorption, and after photocatalysis

Fig. 13 Bar graph representation of (**a**) %adsorption ($t = 60$ min) and (**a**) %degradation ($t = 210$ min) of Methylene blue with PANI, PAZe-1, PAZe-5, PAZe-10, and ZSM-5 (no. of repeat experiments $= 3$)

the conduction band and valance bands in conducting and semiconducting materials, polyaniline possesses the highest occupied molecular orbital (HOMO) and lowest unoccupied molecular orbital (LUMO). Upon photo illumination, electrons get excited from LUMO to HOMO of polyaniline (PANI). These π-π* transitions generate electrons and holes in the valance and conduction band of PANI, respectively. These electrons and holes then induce the formation of active oxidizing species (AOS). The rate of formation of AOS in PANI alone is moderate because of quick electron and hole recombination. ZSM-5 with a bandgap of 2.73 eV, when doped into polyaniline matrices, which has a bandgap of 3 eV, reduces electron–hole combination significantly. When the light bombards the composite material, as ZSM-5 has a bandgap lower than PANI, the electrons from the valance band of ZSM-5 will first excite to its conduction band. Instead of coming back to their own valance band, the electrons jump from the conduction band of ZSM-5 to LUMO of PANI and never go back to its own valance band. Thus, the charge separation increases with a decrease in electron–hole recombination. Ultimately, the rate of formation of AOS increases leading to faster dye degradation. In addition, PANI has a very low tendency to adsorb methylene blue as methylene blue is a cationic dye, and PANI on its surface

has a positive charge. ZSM-5 being negatively charged easily attracts the MB molecule. In a ZSM-5-doped PANI, ZSM-5 adheres the dye molecules on its surface making photocatalysis easier and faster. A schematic of possible mechanism of degradation of methylene blue using ZSM-5 doped PANI is shown in Fig. 14.

Scavenger studies

To analyse the degradation behaviour of methylene blue with ZSM-5/PANI composite PAZe-1, scavenger studies were performed. The purpose of scavenger studies is to find out the responsible species in the degradation mechanism by using a scavenger which binds the respective AOS species and inhibits their activity. Silver nitrate (AgNO₃), disodium EDTA (2Na-EDTA), isopropyl alcohol (IPA), and benzoquinone were used to scavenge the electrons (e^-), holes (h^+), hydroxyl radicals ($OH^•$), and superoxide radicals ($O_2^{•-}$), respectively. For this purpose, 1 mmol of scavenger was added to methylene blue followed by the catalyst prior analysis.

The data in Fig. 15 shows that adding scavengers has reduced the degradation efficiency significantly. By adding AgNO₃, the degradation has reduced by 43.7% which

Fig. 14 Schematic representation of advanced oxidation species formation in ZSM-5-doped polyaniline composite
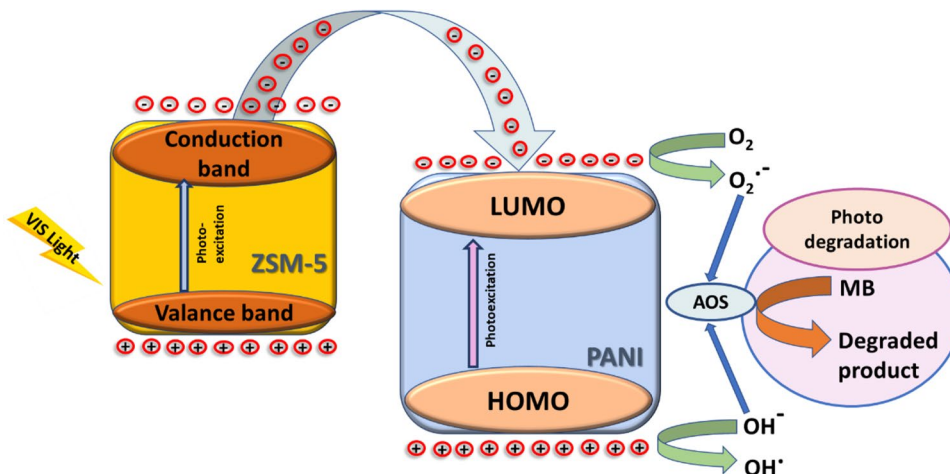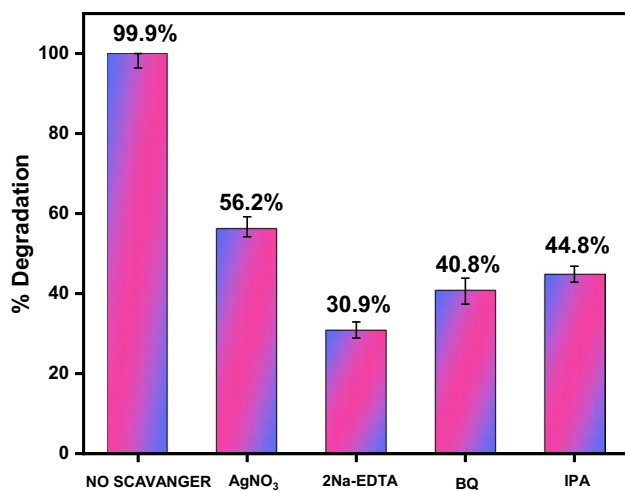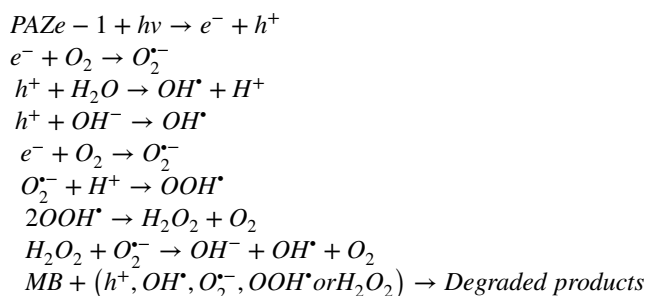
Fig. 15 Effect of scavenger on the degradation of methylene blue using PAZe-1 (no. of repeat experiments = 3)

Fig. 16 Degradation of chlorpyrifos, methyl orange, 2,4-dichlorophenoxy acetic acid, and p-nitroaniline with PAZe-1 photocatalyst (no. of repeat experiments = 3)

indicates that e^- plays a significant role in photocatalysis. Similarly, the addition of disodium EDTA, benzoquinone, and isopropyl alcohol has reduced the degradation to 69%, 59.1%, and 55.1%, respectively. These data show that all four AOS, i.e. electrons (e^-), holes (h^+), hydroxyl radicals ($OH^\bullet$), and superoxide radicals ($O_2^{\bullet-}$) are vital part of the photodegradation mechanism. Based on this analysis, the mechanism of photodegradation can be proposed as below:

$PAZe-1 + hv \rightarrow e^- + h^+$
$e^- + O_2 \rightarrow O_2^{\bullet-}$
$h^+ + H_2O \rightarrow OH^\bullet + H^+$
$h^+ + OH^- \rightarrow OH^\bullet$
$e^- + O_2 \rightarrow O_2^{\bullet-}$
$O_2^{\bullet-} + H^+ \rightarrow OOH^\bullet$
$2OOH^\bullet \rightarrow H_2O_2 + O_2$
$H_2O_2 + O_2^{\bullet-} \rightarrow OH^- + OH^\bullet + O_2$
$MB + \left(h^+, OH^\bullet, O_2^{\bullet-}, OOH^\bullet or H_2O_2 \right) \rightarrow Degraded\ products$

Other organic pollutant degradation studies

The optimized catalyst PAZe-1 was used for the degradation chlorpyrifos, 2,4-dichlorophenoxyacetic acid, methyl orange, and p-nitroaniline. As shown in Fig. 16, the catalyst effectively removed 72% of chlorpyrifos (CPY), 51% of 2,4-dichlorophenoxyacetic acid (2,4 D), 100% of methyl orange, and 26.5% of p-nitroaniline within 15 min.

Stability analysis

To ensure the stability of composite post degradation process, the XRD patterns of optimized composite PAZe-1 were recorded before and after the photocatalysis. For that purpose, the catalyst was washed and dried post analysis and
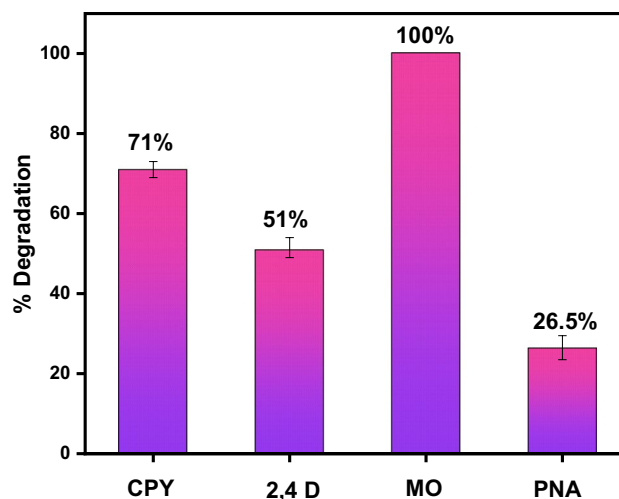
characterized via X-ray diffraction. Figure 17a and b show the XRD patterns of PAZe-1 catalyst before and after photocatalysis. PAZe-1 shows sharp characteristic peak of PANI at 2θ = 25.4°. As the concentration of ZSM-5 in PAZe-1 is very low, the PANI dominates the crystalline nature of ZSM-5, and only peaks of PANI are visible in XRD pattern of PAZe-1. Comparing the two graphs, before and after photocatalysis, the characteristic peak of PANI is still present in both PAZe-1 and PAZe-1 after photocatalysis (APC). The minor peak broadening at 2θ = 25.4° is observed which may be due to slight imperfections in the polycrystalline structure of PANI in the composite. Hence, the XRD stability test suggests that after the one cycle of photodegradation, the catalyst is suitable for further cycles as well.

Comparison of photocatalytic efficiencies (100–150 words)

As stated in Table 1, the degradation results of this experiment were compared to previously published literatures. For this study, 10ppm MB dye was employed with a catalyst dose of 0.5mg/ml. With a visible light irradiation source, 99% methylene blue degradation was achieved within 210 min. Abukhadra et al. examined heulandite/polyaniline composite for LGSF dye degradation with 15ppm dye concentration and 0.5mg/ml catalyst dosage. With visible light irradiation, they found 97% dye degradation in 589 min. A similar experiment was carried out for 20ppm MB, and the percentage degradation achieved was 68.77% with a catalyst dosage of 0.2mg/ml. Similarly, the percentage degradation reported by Liu et al was 93.32%, Abukhadra et al. was 100%, Saha et al. was 30%, Shahabuddin et al. was 88%, Gayatri et al. was 90%, Sboui et al. was 99%, and Sharma et al. was 99.09%. For all the above-stated studies, the

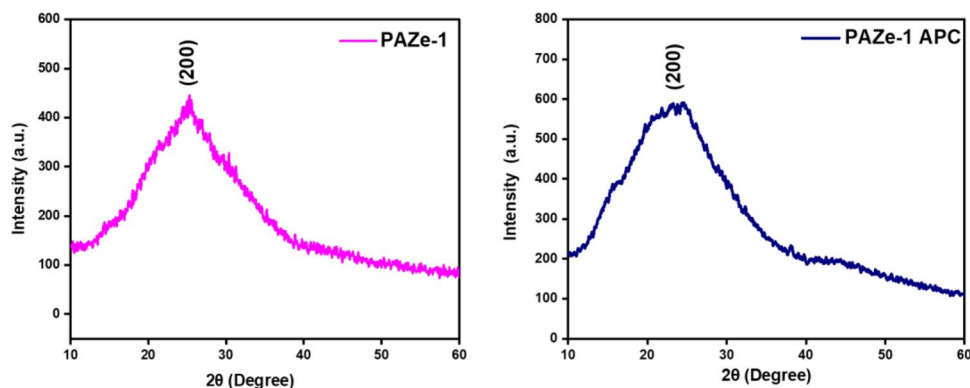**Fig. 17** X-ray diffraction graphs of PAZe-1 before and after photocatalysis

Table 1 Comparison of photocatalytic efficiencies of synthesized material with other reported materials

Photocatalyst	Model contaminant	Dye conc. (mg L^{-1})	Catalyst dosage (mg/ml)	Degradation time (min)	% Degradation	Light source	Ref
Heulandite/polyaniline	LGSF	15 ppm	0.3	589	97%	VIS	Abukhadra et al. (2018a)
Heulandite/polyaniline	MB	20 ppm	0.2	589	68.77%	VIS	Abukhadra et al. (2018a)
TiO_2/zeolite	Sulfadiazine	10 ppm	1	120	93.31%	UV	Liu et al. (2018)
bentonite/PANI@ Ni_2O_3	Safranin-O	5 ppm	0.5	90	100%	Sunlight	Abukhadra et al. (2018b)
PANI/MoS_2	Methylene blue	3.3 ppm	0.1	135	30%	UV	Saha et al. (2019)
Chitosan/PANI/ Co_3O_4	Methylene blue	10 ppm	0.3	180	88%	UV	Shahabuddin et al. (2015)
ZnO/zeolite	Procion red	50 ppm	4	120	90	UV	Gayatri et al. (2021)
TiO_2-PANI/cork	Methyl orange	15	1	210	95	Natural sunlight	Sboui et al. (2017)
PANI/CdS	Rhodamine B	5 ppm	0.5	60	99.09	Visible	Sharma et al. (2016)
This study	Methylene blue	10 ppm	0.5	210	99.9%	VIS	

concentration of the model contaminant was kept between 3 and 20ppm, and the catalyst dose was between 0.1 and 4 mg/ml. Hence, in comparison with previously reported studies, the ZSM-5-doped polyaniline composite has given the better performance and is feasible to use for pollutant degradation.

Future prospective and practical application

The synthesis of composite material is facile and low cost which develops interest for future exploration. The degradation pathway and intermediate products using GC–MS spectroscope can be established. The future research should also be focused on the simultaneous removal of pollutants such as heavy metals, dyes, and agrochemicals. The material from this work can further be explored on large-scale application as a photocatalyst for wastewater treatment as it is cost-effective, efficient, antibacterial, and thermally stable as well. Design and development

of wastewater treatment prototype with the proper functioning of photocatalyst can be done in the future. As discussed earlier, the material is able to remove variety of other contaminants as well; hence, it can be explored for the real-time water treatment. The wastewater treatment system with this material can be established on industrial level and will reduce the difficulties of wastewater handling in countries with developing industrialization.

Conclusion

In situ oxidative polymerization was used to synthesize polyaniline-doped ZSM-5 composites. The Fourier transform infrared (FTIR) data indicated the impregnation of ZSM-5 into polymeric chains of polyaniline. X-ray diffraction (XRD) suggested that ZSM-5 and PAZe-10 have average crystallite sizes of 16.98 nm and 5.91 nm, respectively. Field emission scanning electron microscope indicated the

change in morphology of a polyaniline (PANI) by doping of ZSM-5. The average particle size calculated from FESEM images was found to be 188.24 nm in the case of ZSM-5. The average tube diameter of PANI and PAZe-10 was estimated as 75 nm and 80 nm, respectively. The thermal investigation was carried out by thermo-gravimetric analysis (TGA) which showed that ZSM-5 doping increased the thermal stability of the composites. Photocatalysis was performed under a visible light source with all prepared photocatalysts. Catalyst dosage was kept at 0.5 mg/ml and dye concentration 10 ppm with a contact time of 210 min. The degradation efficiencies for composites PAZe-1, PAZe-5, PAZe-10, and PANI are 99.9%, 82%, and 71, 38%, respectively. In the case of ZSM-5, the total removal was 99%, though ZSM-5 shows adsorption only not photocatalysis, while in the case of ZSM-5-doped PANI composites, ZSM-5 and PANI both work synergistically and show 99% of dye degradation. The PAZe-1 composite also shows 72%, 51%, 100%, and 26.5% removal of chlorpyrifos (CPY), 2,4-dichlorophenoxyacetic acid (2,4 D), methyl orange, and p-nitroaniline within 15 min. The stability analysis via XRD suggests that the composite PAZe-1 is stable enough to employ in multiple cycles. Hence, the facile synthesis of materials and simple visible-light-driven degradation approach can easily be used for environmental remediation.

Declarations

Ethics approval and consent to participate Not applicable.

Consent for publication Not applicable.

Competing interests The authors declare no competing interests.

References

Abukhadra MR, Rabia M, Shaban M, Verpoort F (2018a) Heulandite/polyaniline hybrid composite for efficient removal of acidic dye from water; kinetic, equilibrium studies and statistical optimization. Adv Powder Technol 29:2501–2511

Abukhadra MR, Shaban M, Sayed F, Saad I (2018b) Efficient photocatalytic removal of safranin-O dye pollutants from water under sunlight using synthetic bentonite/polyaniline@ Ni2O3 photocatalyst of enhanced properties. Environ Sci Pollut Res 25:33264–33276

Akti F, Okur M (2018) The removal of acid violet 90 from aqueous solutions using PANI and PANI/clinoptilolite composites: isotherm and kinetics. J Polym Environ 26:4233–4242

Alberti S, Basciu I, Vocciante M, Ferretti M (2021) Experimental and physico-chemical comparison of ZnO nanoparticles' activity for photocatalytic applications in wastewater treatment. Catalysts 11:678

Alshameri A, Ibrahim A, Assabri AM, Lei X, Wang H, Yan C (2014) The investigation into the ammonium removal performance of Yemeni natural zeolite: modification, ion exchange mechanism, and thermodynamics. Powder Technol 258:20–31

Alswat AA, Ahmad MB, Saleh TA (2016) Zeolite modified with copper oxide and iron oxide for lead and arsenic adsorption from aqueous solutions. J Water Supply Res Technol Aqua 65:465–479

Alvarez-Aguinaga EA, Elizalde-González MP, Sabinas-Hernandez SA (2020) Unpredicted photocatalytic activity of clinoptilolite–mordenite natural zeolite. RSC Adv 10:39251–39260

Armağan B, Turan M (2004) Equilibrium studies on the adsorption of reactive azo dyes into zeolite. Desalination 170:33–39

Danish M, Tayyab M, Akhtar A, Altaf AA, Kausar S, Ullah S, Iqbal M (2020) Effect of soft template variation on the synthesis, physical, and electrochemical properties of Mn3O4 nanomaterial. Inorg Nano-Metal Chem 51:359–365

Darban Z, Shahabuddin S, Gaur R, Ahmad I, Sridewi N (2022) Hydrogel-based adsorbent material for the effective removal of heavy metals from wastewater: a comprehensive review. Gels 8:263

Delanka-Pedige H, Zhang Y, Nirmalakhandan N (2022) Algal wastewater treatment integrated with carbon adsorption and ozonation for water reclamation: multi-criteria comparison with conventional pathways. Algal Res 61:102581

Domingues E, Fernandes E, Gomes J, Castro-Silva S, Martins RC (2021) Olive oil extraction industry wastewater treatment by coagulation and Fenton's process. J Water Process Eng 39:101818

Gayatri R, Agustina TE, Moeksin R, Bahrin D, Gustini G (2021) Preparation and characterization of ZnO-zeolite nanocomposite for photocatalytic degradation by ultraviolet light. J Ecol Eng 22:178–186

Gupta S, Nayak A, Roy C, Yadav AK (2021) An algal assisted constructed wetland-microbial fuel cell integrated with sand filter for efficient wastewater treatment and electricity production. Chemosphere 263:128132

Jha S, Gaur R, Shahabuddin S, Ahmad I, Sridewi N (2022) Kinetic and isothermal investigations on the use of low cost coconut fiber-polyaniline composites for the removal of chromium from wastewater. Polymers 14:4264

Khan A, Hussain R, Toufiq AM, Shah A, Khan BA, Niazur Rahman ZS (2020) Fabrication of cryptomelane FexMn1-xO2 with enhanced antibacterial activity and specific heat capacity. Mater Charact 169:110661

Li Y, Yu H, Liu L, Yu H (2021) Application of co-pyrolysis biochar for the adsorption and immobilization of heavy metals in contaminated environmental substrates. J Hazard Mater 420:126655

Liu X, Liu Y, Lu S, Guo W, Xi B (2018) Performance and mechanism into TiO2/Zeolite composites for sulfadiazine adsorption and photodegradation. Chem Eng J 350:131–147

Liu G, Feng M, Tayyab M, Gong J, Zhang M, Yang M, Lin K (2021a) Direct and efficient reduction of perfluorooctanoic acid

using bimetallic catalyst supported on carbon. J Hazard Mater 412:125224

Liu Y, Zhu Q, Tayyab M, Zhou L, Lei J, Zhang J (2021b) Single-atom Pt loaded zinc vacancies ZnO–ZnS Induced type-v electron transport for efficiency photocatalytic H2 evolution. Solar Rrl 5:2100536

Makuła P, Pacia M, Macyk W (2018) How to correctly determine the band gap energy of modified semiconductor photocatalysts based on UV–Vis spectra. J Phys Chem Lett 9(23):6814–6817

Mehmood S, Ahmed W, Ikram M, Imtiaz M, Mahmood S, Tu S, Chen D (2020) Chitosan modified biochar increases soybean (Glycine max L.) resistance to salt-stress by augmenting root morphology, antioxidant defense mechanisms and the expression of stress responsive genes. Plants 9:1173

Mehmood S, Ahmed W, Rizwan M, Imtiaz M, Elnahal ASMA, Ditta A, Irshad S, Ikram M, Li W (2021) Comparative efficacy of raw and HNO3-modified biochar derived from rice straw on vanadium transformation and its uptake by rice (Oryza sativa L) insights from photosynthesis, antioxidative response, and gene-expression profile. Environ Pollut 289:117916

Mehmood S, Ahmed W, Alatalo JM, Mahmood M, Imtiaz M, Ditta A, Ali EF, Abdelrahman H, Slaný M, Antoniadis V (2022) Herbal plants-and rice straw-derived biochars reduced metal mobilization in fishpond sediments and improved their potential as fertilizers. Sci Total Environ 826:154043

Narayanan S, Judith Vijaya J, Sivasanker S, John Kennedy L, Ariharan A (2014) Enhanced selectivity to benzaldehyde in the liquid phase oxidation of benzyl alcohol using nanocrystalline ZSM-5 zeolite catalyst. J Porous Mater 21:633–641

Narayanan S, Vijaya JJ, Sivasanker S, Kennedy LJ, Jesudoss S (2015) Structural, morphological and catalytic investigations on hierarchical ZSM-5 zeolite hexagonal cubes by surfactant assisted hydrothermal method. Powder Technol 274:338–348

Ownby M, Desrosiers D-A, Vaneeckhaute C (2021) Phosphorus removal and recovery from wastewater via hybrid ion exchange nanotechnology: a study on sustainable regeneration chemistries. NPJ Clean Water 4:1–8

Parekh K, Radadiya R, Gaur R, Shahabuddin S, Ahmad I (2022) A cost-effective approach for decontamination of used lubricant oil: enhanced recovery of base oil using different adsorbents. Int J Environ Sci Technol 1–20. https://doi.org/10.1007/s13762-022-04676-w

Saha S, Chaudhary N, Mittal H, Gupta G, Khanuja M (2019) Inorganic–organic nanohybrid of MoS2-PANI for advanced photocatalytic application. Int Nano Lett 9:127–139

Sboui M, Nsib MF, Rayes A, Swaminathan M, Houas A (2017) TiO2–PANI/cork composite: a new floating photocatalyst for the treatment of organic pollutants under sunlight irradiation. J Environ Sci 60:3–13

Sessarego S, Rodrigues SC, Xiao Y, Lu Q, Hill JM (2019) Phosphonium-enhanced chitosan for Cr (VI) adsorption in wastewater treatment. Carbohyd Polym 211:249–256

Shahabuddin S, Sarih NM, Ismail FH, Shahid MM, Huang NM (2015) Synthesis of chitosan grafted-polyaniline/Co 3 O 4 nanocube nanocomposites and their photocatalytic activity toward methylene blue dye degradation. RSC Adv 5:83857–83867

Shahabuddin S, Muhamad Sarih N, Mohamad S, Joon Ching J (2016) SrtiO3 nanocube-doped polyaniline nanocomposites with enhanced photocatalytic degradation of methylene blue under visible light. Polymers 8:27

Sharma S, Singh S, Khare N (2016) Synthesis of polyaniline/CdS (nanoflowers and nanorods) nanocomposites: a comparative study towards enhanced photocatalytic activity for degradation of organic dye. Colloid Polym Sci 294:917–926

Shi L, Wang X, Lu L, Yang X, Wu X (2009) Preparation of TiO2/polyaniline nanocomposite from a lyotropic liquid crystalline solution. Synth Met 159:2525–2529

Shkir M, Palanivel B, Khan A, Kumar M, Chang J-H, Mani A, AlFaify S (2022) Enhanced photocatalytic activities of facile auto-combustion synthesized ZnO nanoparticles for wastewater treatment: an impact of Ni doping. Chemosphere 291:132687

Tagliabue M, Rizzo C, Onorati NB, Gambarotta EF, Carati A, Bazzano F (2012) Regenerability of zeolites as adsorbents for natural gas sweetening: a case-study. Fuel 93:238–244

Tayyab M, Liu Y, Liu Z, Pan L, Xu Z, Yue W, Zhou L, Lei J, Zhang J (2022a) One-pot in-situ hydrothermal synthesis of ternary In2S3/Nb2O5/Nb2C Schottky/S-scheme integrated heterojunction for efficient photocatalytic hydrogen production. J Colloid Interface Sci 628:500–512

Tayyab M, Liu Y, Min S, Irfan RM, Zhu Q, Zhou L, Lei J, Zhang J (2022b) Simultaneous hydrogen production with the selective oxidation of benzyl alcohol to benzaldehyde by a noble-metal-free photocatalyst VC/CdS nanowires. Chin J Catal 43:1165–1175

Younis SA, Serp P, Nassar HN (2021) Photocatalytic and biocidal activities of ZnTiO2 oxynitride heterojunction with MOF-5 and g-C3N4: a case study for textile wastewater treatment under direct sunlight. J Hazard Mater 410:124562

Zhou M, Rownaghi AA, Hedlund J (2013) Synthesis of mesoporous ZSM-5 zeolite crystals by conventional hydrothermal treatment. RSC Adv 3:15596–15599